

FUTPRINT50 Academy

HA I Q U

FUTPRINT50 Design Challenge



Submitted on September 2nd 2022

Team Members: Jona Eissele, Stefan Lafer, Cristian Mejía-Burbano,
Julian Schließus, Tristan Wiedmann

Academic Supervision: Prof. Dr. Andreas Strohmayer, M. Sc. Jonas Mangold

HAIQU



FUTPRINT5  Academy

Disclaimer FUTPRINT50 Academy

This research project has received funding from the European Union's Horizon 2020 research and innovation programme under grant agreement No 875551.

The findings presented here have been studied, acquired and prepared by the student teams independently. The teams were able to obtain support from the expertise of the FUTPRINT50 Consortium. However, the statements made herein do not necessarily have the consent or agreement of the FUTPRINT50 Consortium. These represent the opinion and investigations of the author(s).

Copyright © 2022, FUTPRINT50 Consortium, all rights reserved.

This document and its contents remain the property of the beneficiaries of the FUTPRINT50 Consortium. It may contain information subject to intellectual property rights. No intellectual property rights are granted by the delivery of this document or the disclosure of its content. Reproduction or circulation of this document to any third party is prohibited without the consent of the author(s).

THIS DOCUMENT IS PROVIDED BY THE COPYRIGHT HOLDERS AND CONTRIBUTORS "AS IS" AND ANY EXPRESS OR IMPLIED WARRANTIES, INCLUDING, BUT NOT LIMITED TO, THE IMPLIED WARRANTIES OF MERCHANTABILITY AND FITNESS FOR A PARTICULAR PURPOSE ARE DISCLAIMED. IN NO EVENT SHALL THE COPYRIGHT OWNER OR CONTRIBUTORS BE LIABLE FOR ANY DIRECT, INDIRECT, INCIDENTAL, SPECIAL, EXEMPLARY, OR CONSEQUENTIAL DAMAGES (INCLUDING, BUT NOT LIMITED TO, PROCUREMENT OF SUBSTITUTE GOODS OR SERVICES; LOSS OF USE, DATA, OR PROFITS; OR BUSINESS INTERRUPTION) HOWEVER CAUSED AND ON ANY THEORY OF LIABILITY, WHETHER IN CONTRACT, STRICT LIABILITY, OR TORT (INCLUDING NEGLIGENCE OR OTHERWISE) ARISING IN ANY WAY OUT OF THE USE OF THIS DOCUMENT, EVEN IF ADVISED OF THE POSSIBILITY OF SUCH DAMAGE.

Abstract

In recent years, the rapid growth of air transportation and therefore the rise in air pollution and greenhouse gas emissions has generated a need for sustainable propulsion concepts in aviation. Therefore, hybrid-electric aviation propulsion technologies promise an environmentally friendly solution to meet the Paris Climate Agreement. As a contribution to the reduction of aircraft emissions, the design team of the University of Stuttgart is proud to present their concept HAIQU for a sustainable regional aircraft as entry to the FUTPRINT50 Aircraft Design Challenge 2022. Benefiting from technological progress, this aircraft provides a sustainable solution for future air transport in the regional sector. This study assesses the efficiency advantages arising from the integration of a hybrid-electric powertrain with hydrogen powered fuel cells. In addition to the liquid fuel electric batteries are used for secondary energy storage to supply the required power for takeoff. Hereby the future rise of the conventional jet fuel price as well as possible penalties on emissions were taken into account.

HAIQU uses liquid hydrogen as main energy carrier, which is stored in two tanks behind the rear bulkhead. The liquid hydrogen is used to cool the major components while also being heated to the optimal processing temperature, harvesting synergetic effects. The power electronics as well as the main power cables and the motors use superconducting technologies to increase efficiency. The efficiency is further enhanced by the deployment of wingtip propellers and an electric green taxiing system, significantly reducing fuel consumption. The combination of the fuel type and the high efficiencies result in a change of design point compared to the top-level aircraft requirements, which is elegantly dealt with to keep similar operational possibilities compared to current aircraft. Trade-off studies were conducted regarding the hybridization, wingspan, and the power split between the propellers. Each one resulted in an improved overall aircraft.

Two major focal points of the design were the direct operating costs as well as the turnaround time. The goal was to reduce costs and have no negative effect on the turnaround with the hybrid powertrain. Both of those goals are achieved. The resulting design of HAIQU has improved efficiency, increasing passenger comfort and overall much less emission compared to current aircraft, resulting in a good step towards climate neutral aviation.

Keywords: FUTPRINT50, Design Challenge, Climate Impact, Aircraft Design Concept, Hybrid

Contents

Disclaimer FUTPRINT50 Academy	II
Abstract	III
Contents	V
Abbreviation	VII
List of Figures	IX
List of Tables	X
1 Introduction	1
1.1 Aircraft Requirements	1
1.2 Reference Aircraft	2
1.3 HAIQU	2
2 Architecture of HAIQU	2
2.1 Configuration Selection	2
2.2 Propulsion System and Powertrain	3
3 Aircraft Components	9
3.1 Proton Exchange Membrane Fuel Cell	9
3.2 Liquid Hydrogen Fuel Tanks	9
3.3 Battery	11
3.4 Electric Motor	12
3.5 Propeller	12
3.6 Fuselage	13
3.7 Wing	14
3.8 Empennage	15
3.9 Landing Gear	15
3.10 Electric Green Taxiing System	15
4 Performance and Technical Data	16
4.1 Payload-Range diagram	16
4.2 Performance Characteristics	18
4.3 Mass Estimation	18
4.4 Turnaround Process	19
4.5 Sustainability	22
5 Direct Operating Costs	23
5.1 Assumptions	23
5.2 Resulting Cost for Design Mission	23
5.3 Resulting Cost for Benchmark Mission	24
6 Conclusion	25

Contents

References	26
7 Appendix A – Three Side View	31
8 Appendix B -Technical Summary	32

Abbreviation

AEA	Association of European Airlines
BLI	Boundary Layer Ingestion
CO ₂	Carbon Dioxide
DC/AC	Direct Current to Alternating Current
DC/DC	Direct Current to Direct Current
DEP	Distributed Electric Propulsion
EGTS	Electric Green Taxiing System
ESS	Energy Storage System
ETDS	Electric Traction Drive System
Fig.	Figure
FRP	Fiber Reinforced Plastic
FUTPRINT50	FUTURE PROpulsion & INTegration: towards a hybrid-electric 50-seat regional aircraft
H ₂	Hydrogen
HAIQU	H ydrogen A ircraft designed for Q uick comm U ting
HTS cables	High Temperature Semiconducting cables
APU	Auxiliary Power Unit
LCO	Lithium Cobalt Oxide (LiCoO ₂)
LFP	Lithium Iron Phosphate (LiFePO ₄)
LH ₂	Liquid Hydrogen
MAC	Mean Aerodynamic Chord
MTOM	Maximum Take-Off Mass
NMC	Lithium Nickel Manganese Cobalt Oxide (LiNiMnCoO ₂)
NO _x	Nitrogen Oxides

Abbreviation

OME	Operating Mass Empty
PEMFC	Proton Exchange Membrane Fuel Cell
SAF	Sustainable Aviation Fuel
SCM	Super Conducting Motor
SoA	State of the Art
SOC	State of Charge
SOFC	Solid Oxide Fuel Cell
Tab.	Table
TLAR	Top-Level Aircraft Requirements
TMS	Thermal Management System
TRL	Technology Readiness Level
WTP	Wing Tip Propeller

List of Figures

Figure 2-1: Graphic Synopsis of the configurations investigated, the configurations in green were subjected to a detailed tradeoff study on the aircraft level.....	2
Figure 2-2: Powertrain Architecture of HAIQU: The fuel tanks supply the 2 PEMFCs with H ₂ , which then provide power together with two batteries to the converters that supply the motors. There are two motors with gearboxes and propellers on each wing, one on the wingtip and one close to the body	5
Figure 2-3: Sizing diagram of HAIQU calibrated with the reference aircraft. The design point is limited by the stall speed and takeoff distance.....	6
Figure 2-4: Operating conditions for takeoff, cruise and descend on the PEMFC polarization curve	6
Figure 2-5: Detailed representation of the powertrain model.....	7
Figure 2-6: Flow chart of hydrogen in the TMS.....	8
Figure 3-1: Shape and location of LH ₂ tanks.....	10
Figure 3-2: Snapshot of LFP, LCO and NMC batteries comparison.....	11
Figure 3-3: Specific power vs. specific energy of Li-Ion batteries distinguished by cell chemistry	11
Figure 3-4: Cross-section of HAIQU showcasing the two sections. The lower section in grey houses the TMS, electronics and the gear while the upper section houses the cabin.....	13
Figure 3-5: Cabin Layout of HAIQU	14
Figure 4-1: Payload-Range-Diagram comparison.....	17
Figure 4-2: Gantt-Chart of the Turnaround Process.....	20
Figure 5-1: Cost for Design Mission for HAIQU based in 1509 flights per year	24
Figure 5-2: Direct operation cost from reference aircraft and HAIQU based in 1810 flights per year.....	25

List of Tables

Table 1-1: Top Level Aircraft Requirements 1

Table 3-1: Power requirements for PEMFC 9

Table 3-2: EGTS-dimensions and TRL.....16

Table 4-1: Main performance characteristics of HAIQU18

Table 4-2: Mass of components19

Table 4-3: Mass estimation for new Design Mission (400km @ 5800 kg)19

1 Introduction

This technical report presents the findings of the aircraft design team of the University of Stuttgart for the FUTPRINT50 Design Challenge. The requirements given were very limited to give the students a lot of freedom to explore new technologies, those used by the team are presented in the following chapters.

In this chapter firstly, the aircraft requirements provided by the FUTPRINT50 Academy are listed, then the reference aircraft is addressed and finally the HAIQU name is explained.

1.1 Aircraft Requirements

TLAR	Value
Number of passengers	50
Passenger weight	106 kg per Passenger (incl. luggage) = 5300 kg
Design range	800 km
Design cruise speed	\leq Ma 0.48
Maximum payload	5800 kg
Reserve fuel policy	185 km + 30 min holding
Rate of climb (MTOM, SL, ISA)	\geq 1850 ft/min
Time to climb to FL 170	\geq 13 min
Maximum operating altitude	7620 m (25000ft)
Take-off field length	\leq 1000 m
Landing field length	\leq 1000 m
Benchmark for DOCs	Design payload with 400 km mission

Table 1-1: Top Level Aircraft Requirements [1]

The Top-Level Aircraft Requirements (TLAR) are defined by the FUTPRINT50 committee [1] and listed in Table 1-1. Most of these parameters fit a typical regional aircraft design. The significant difference is the short design range compared to an ATR 42-600 [2]. In addition, the benchmark range is set to 400 km based on actual flown distances.

1.2 Reference Aircraft

The ATR 42 family includes the 300, 320, 400, 500 and 600 series. Those aircrafts do all have the same dimensions and differ on the usage and performance [3]. The latest ATR 42 – 600 is set as the main reference aircraft. Except for the latest presented version (ATR 42-600S), the short takeoff and landing field length of 1000 m cannot be met by the other versions [4]. The required design range of 800 km from the TLARs is about 60 % of the reference aircraft [3]. All remaining requirements varies not significant.

1.3 HAIQU

The name of the aircraft design of the team of the Universität Stuttgart is HAIQU. It is the short form of **H**ydrogen **A**ircraft **d**esigned for **Q**uick comm**U**ting. The name is inspired by the traditional Japanese short poem form Haiku. The “Quick Commuting” is enabled by the Electric Green Taxing System (EGTS), the fast refueling and recharging ability during the turnaround process.

2 Architecture of HAIQU

In the following sections the decision making between different technological approaches and the general architecture of HAIQU is going to be explained.

2.1 Configuration Selection

In Figure 2-1 all analyzed design possibilities are listed. Each design possibility is evaluated by the same criterions rated between zero (inadequate) and five (excellent) points [5].

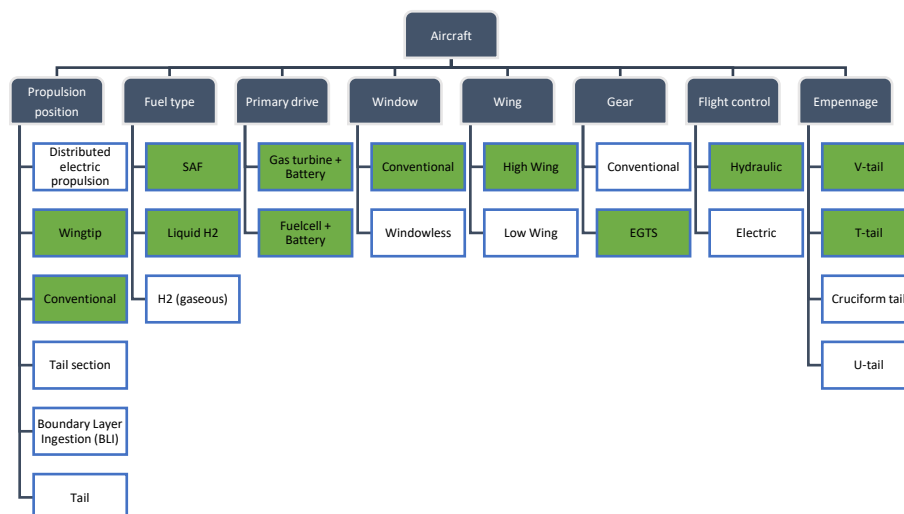


Figure 2-1: Graphic Synopsis of the configurations investigated, the configurations in green were subjected to a detailed tradeoff study on the aircraft level

2 Architecture of HAIQU

The blue boxes represent the components on which different technologies were addressed for their respective improvement. The list of possible technologies was organized under each of the areas to be listed. The green color constitutes the design opportunities where the technological improvements are implemented. Different trade-off studies were conducted in order to investigate the effects on the entire aircraft while varying different components to elaborate the best configuration.

In the following section the final propulsion design choice is evaluated by a detailed case study and calculations with the developed design program.

2.2 Propulsion System and Powertrain

The selection of propulsion configuration and engines represents one of the most important features in aircraft design. The selection of the configuration will have implications in the selection of the propulsion components and the materials of the aircraft to obtain the highest possible efficiency and the reduction of emissions and noise. Two main types of considered propulsion configurations are [6]:

1. Turbo-Hybrid Electric Propulsion System
2. Fuel-Cell Propulsion System

The two technologies represent the most optimal alternatives for the propulsion system and powertrain that have the greatest opportunity for operation in subsequent years. The main criteria are supported by recent research in the aeronautical industry where optimization of performance, environmental impact and costs are sought [7]. The predominant evaluation and decision criteria for the choice of propulsion system are described below.

2.2.1 Turbo-Hybrid Electric Propulsion System

Electric turbo-hybrid propulsion systems are developed as alternatives to the purely electric battery propulsion system as a measure to supplement the currently low energy density of batteries. These types of systems add different power generators to the battery system with versatility for different types of components and configurations. Propulsion generators such as fans or propellers can be driven by the electric motor alone (serial-hybrid concept) or by the electric motor and gas turbine together (parallel-hybrid concept) [8]. Current aircraft have their gas turbines dimensioned by the need for sufficient power at take-off to achieve desired take-off field lengths and sufficient safety margins if a turbine were to fail. During cruise and climb the turbine is not running at maximum power, which results in unused potential and demands a bigger trade-off between power and efficiency, since the two relevant scenarios require a largely different thrust setting [9].

The hybrid propulsion concept bridges this gap by using a secondary energy source, e.g., a battery, to supply the peak power. During cruise the battery is not used, and the turbine can run within a small performance window the whole flight. This makes it possible to optimize the gas turbine more than in conventional use. The secondary effect is a weight reduction of the turbine because it must provide less max. power. This effect is mitigated by the extra weight of the hybrid drivetrain and the secondary energy source [10].

2.2.2 Fuel Cell Hybrid-Electric Propulsion System

A fuel cell is a type of technology for power generation through the conversion of chemical potential energy to electrical energy through the reaction between hydrogen and oxygen [11]. There are basically two types of fuel cells, such as the Solid Oxide Fuel Cell (SOFC) and the Proton Exchange Membrane Fuel Cell (PEMFC). Due to the maturity, high power-to-weight ratio and short reaction time PEMFC is the most promising technology in aviation sector over SOFC [12]. Batteries could serve as a complement to supplement the low power-to-weight ratio of fuel cells (1-2 kW/kg) compared to gas turbines (5-15 kW/kg) and mitigate the slow response of the fuel cell [13]. New technologies however show that a performance of about 6 kW/kg is possible to reach in the core of the system. The main advantage of fuel cells compared to gas turbines is the supply of energy through catalytic reaction, which implies zero emission of CO₂, Soot or NO_x with an efficiency of 50 % [10]. The main challenge of this technology is the storage of hydrogen and the cooling of the fuel cell. It has been shown to be possible at smaller aircraft level already and there are projects running by Deutsche Aircraft and H2fly, Zeroavia and MTU at increasing aircraft sizes [14] [15] [16].

2.2.3 Decision

After a detailed case study, the Fuel Cell Hybrid-Electric Propulsion system was selected because it had the lowest total weight, lower energy consumption, lower fuel prices as well as the lowest emissions for the given timeframe. Those advantages stem mostly from the use of LH₂ as primary energy carrier. Its high gravimetric density combined with the very low emissions make it more suitable and cheaper to fulfill the TLAR for this specific case. Another factor, that is neither aircraft nor airport relevant is the lower amount of energy required to produce the same amount of hydrogen energy compared to SAF energy [14]. This improves the socio-economic attributes of HAIQU. The downside is the increased complexity and the number of new technologies used, but the advantages were unanimously biased towards this concept. The architecture can be seen in Figure 2-2. The full three-side view can be found in Appendix A.

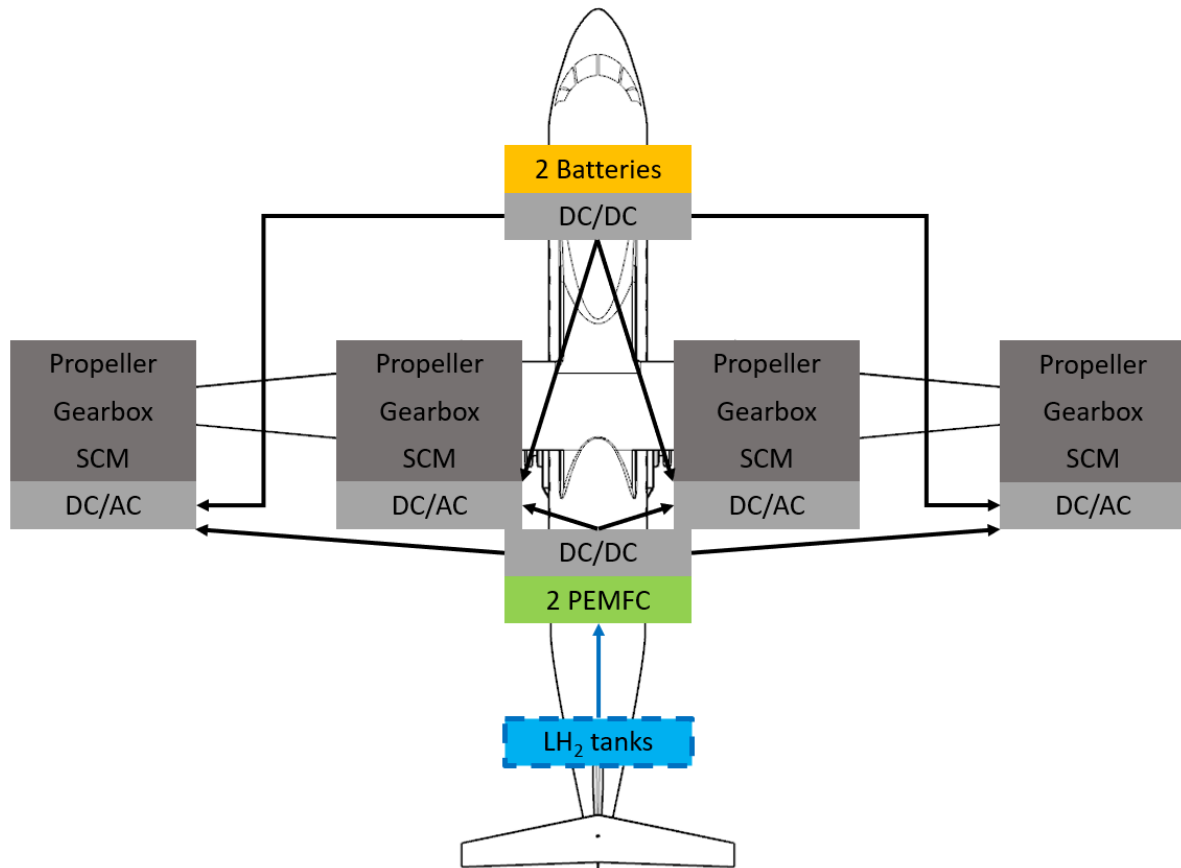


Figure 2-2: Powertrain Architecture of HAIQU: The fuel tanks supply the 2 PEMFCs with H₂, which then provide power together with two batteries to the converters that supply the motors. There are two motors with gearboxes and propellers on each wing, one on the wingtip and one close to the body

2.2.4 Aircraft Sizing Chart

Figure 2-3 shows the sizing diagram of HAIQU. The choice of the design point is mainly limited by the stall speed and the takeoff distance of the airplane. While the design point of the reference aircraft is limited by the engine power, HAIQU can profit from scalable electric engine technology which allows a design at higher power loading and thus higher wing loading. Therefore, a heavier hybrid powertrain can be integrated while maintaining an equivalent wing area.

In order to increase the accuracy of the sizing chart, the design program was calibrated with the data from the reference aircraft. For calibration, the dimensions and masses from Janes [17] for the reference aircraft are used. The wing loading of 361 kg/m² and the power loading of 20 W/N describe the design point of HAIQU.

2 Architecture of HAIQU

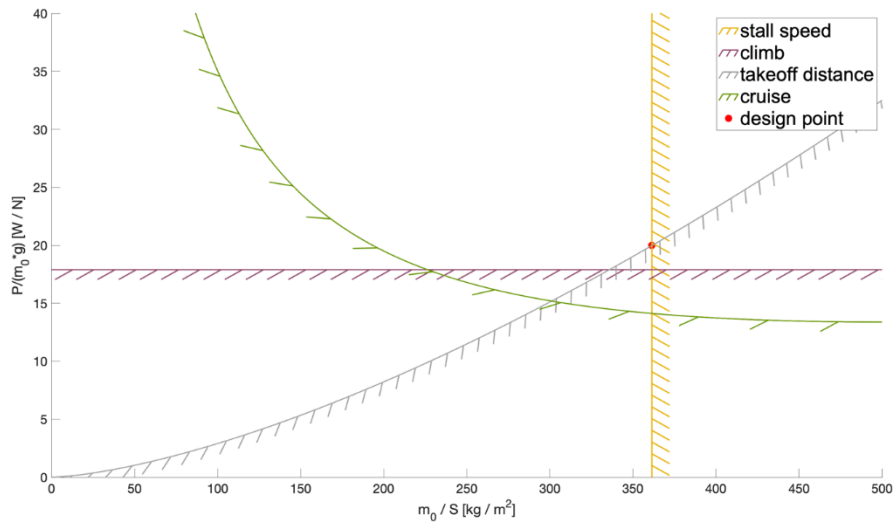


Figure 2-3: Sizing diagram of HAIQU calibrated with the reference aircraft. The design point is limited by the stall speed and takeoff distance.

2.2.5 Detailed Architecture

The aircraft is mainly powered by two identical PEMFC that each provide 44 % of the maximum takeoff power. This split is defined by the required energy during cruise since it is the longest phase of the mission and the most critical regarding efficiency. The remaining 12 % of takeoff power are supplied by the two batteries. For the other mission segments the fuel cells are operated at power levels above their most efficient point of operation. This makes them less efficient but reduces the required size of the batteries, which are less energy dense than the PEMFC system. Two PEMFC are used to create redundancy required by CS-25 (EASA Certification Specification-25).

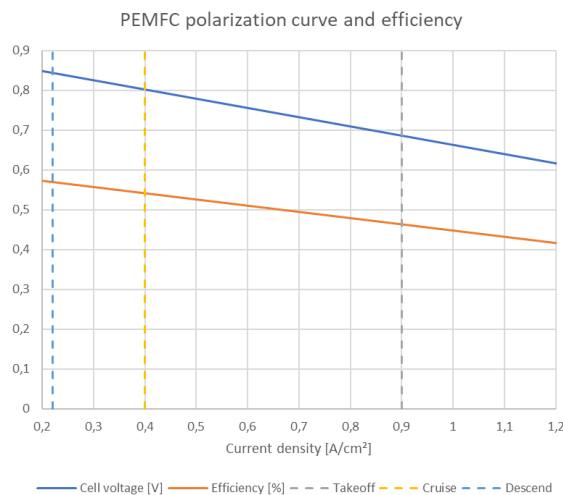


Figure 2-4: Operating conditions for takeoff, cruise and descend on the PEMFC polarization curve; gradients taken from Hartmann et al. [18]

2 Architecture of HAIQU

The two batteries are only providing power in phases where high power is critical. This refers to takeoff, climb and emergency situations, for example the malfunction of one of the two fuel cells. The detailed use of the battery system will be further elaborated in chapter 3.3 and 4.4.1. A diagram of the energy flow in the propulsion system can be seen in Figure 2-5.

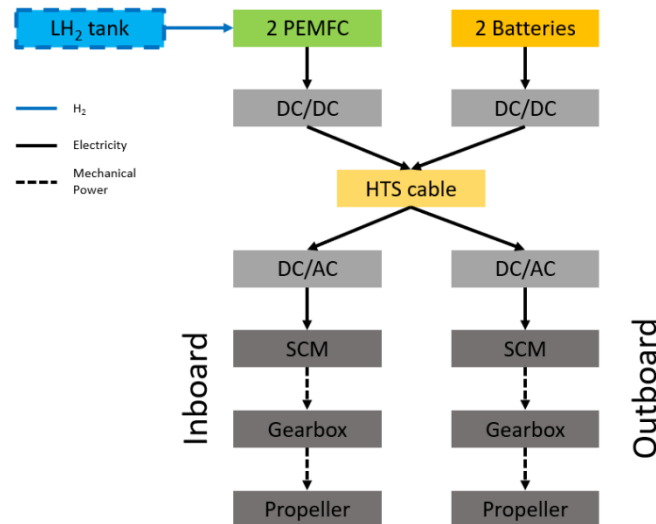


Figure 2-5: Detailed representation of the powertrain model, created by Hartmann et al. [18], adjusted to fit HAIQU

The electric power provided by the PEMFC system and the batteries is then transformed by a DC/DC converter each to reach the optimum voltage for the use of high temperature semiconducting cables (HTS cables). Those run from the DC/DC converters to the superconducting motors (SCM) where the electric power is transformed by DC/AC converters. The SCM are then coupled to a planetary gearbox that transforms the high rpm of the motor to the low desired speed of the propellers. Since the powertrain components need cooling and the liquid hydrogen needs heating to be processable by the PEMFC a synergetic use developed by Hartmann et. al. [18] is used in HAIQU.

The PEMFC are provided with air that is compressed, cooled, and humidified before it arrives at the stacks. Within this cycle the condensed water from the exhaust of the fuel cell is partially reused to humidify the air, the rest is discarded outside of the aircraft.

2.2.6 Thermal Management System (TMS)

The TMS is an integral part of the hybrid aircraft. Because the temperature differences between atmosphere and heat generating components is quite low, with battery temperatures in the range of 315 K and PEMFC temperatures at about 358 K the efficiency of the heat exchange is quite low, resulting in high TMS masses and dimensions. Furthermore, the maximum thermal load occurs during takeoff and climb, where the speed is low, and temperatures are relatively high. The use of ram air-based thermal management systems allows a fan to be used

2 Architecture of HAIQU

during low-speed phases of the mission as suggested by Hartmann et al. [18]. Those systems are examined in further detail in other studies [19] [20].

To provide sufficient cooling for the hydrogen-cooled components a minimal mass-flowrate must be maintained [18]. This must be consumed by the PEMFC to use the hydrogen, resulting in a minimal required power setting. The flow of the hydrogen is visualized in Figure 2-6:

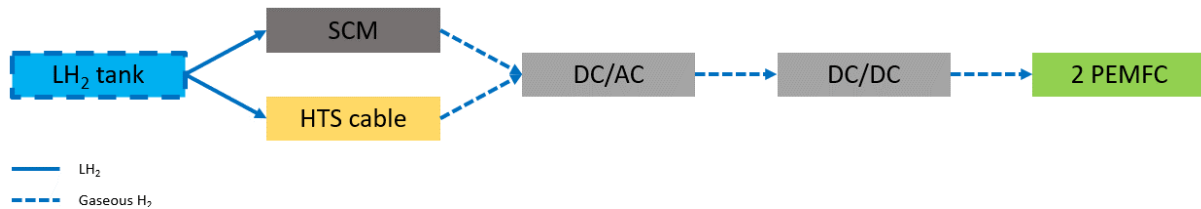


Figure 2-6: Flow chart of hydrogen in the TMS, developed by Hartmann et al. [18], adjusted to HAIQU

The hydrogen is firstly used to cool the four SCM. Hartmann et al. [18] suggest cooling the HTS cables next, but in the configuration of HAIQU with Wing Tip Propulsion (WTP) it would be necessary to route the hydrogen from the wingtips back to the center of the aircraft and back to the DC/AC converters in the wingtip. This would be too much piping and increase the weight of the system as well as the losses in transport. Therefore, HAIQU uses two parallel LH₂ streams from the tank to the SCM and through the HTS cable. The two streams connect again at the DC/AC converters where the output temperature is somewhere in between 80 and 100 K, reducing the losses for the transport back to the center of the aircraft compared to the 65 K after the SCM.

At the center of the aircraft the hydrogen is used to cool the DC/DC converters and lastly will be heated using the PEMFC to reach 358 K as optimal input temperature. The hydrogen alone is not enough to cool all components as it only provides 4 % of the cooling need of the PEMFC [18].

The ram-air based TMS must remove about 760 kW of heat from the PEMFC and SCM combined [18]. Applying the ratio of required power to removed heat from Chapman et al. [20] the resulting TMS power requirement was included in the aircraft power requirements at cruise. The ram-air cooling components are positioned in the belly of the aircraft, located forward of the main landing gear. The drag increase from the TMS is estimated between 0.3 % and 0.7 % by Kellermann et al. [19]. Those losses were however determined for a faster aircraft at Ma = 0.68. The design of the TMS makes use of the so-called Meredith effect, resulting in a drag decrease compared to simplistic TMS designs [21]. For low-speed phases of the flight and taxiing a pulling fan is installed in the TMS to increase the airflow and provide sufficient cooling for the PEMFC [20].

3 Aircraft Components

The aircraft consists of many components but only the most important ones are described in the following chapters, justifying the components selection, presenting the sizing methodology and listing the results of the trade-off studies.

3.1 Proton Exchange Membrane Fuel Cell

The PEMFC has many requirements to fulfill that influence the sizing. First, it must provide sufficient power by itself for cruise and climb to reduce the battery size. Second, it must provide sufficient power at takeoff to reduce the size of the battery which is boosting the power in this phase. Third, it must operate at high efficiencies to firstly reduce fuel consumption and secondly reduce the heat generated. And last, it must consume the minimal H₂ mass flow for the hydrogen cooling to prevent the venting of excess H₂. Those requirements are listed in Table 3-1:

Scenario	Required Power
Climb	2700 kW
Cruise	1800 kW
Take-off	3100 kW
Minimal power for cooling flow	1000 kW

Table 3-1: Power requirements for PEMFC

The powers for take-off, climb and cruise are calculated using an incremental simulation over the whole flight mission, considering kinetic and potential energy, drag, and efficiencies. The minimal power is calculated using the values for the investigated aircraft by Hartmann et al. [18] regarding cruise power and efficiency and calculating the resulting mass-flow of H₂. This mass-flow is extrapolated using the cruise power to HAIQU and transformed into a minimal power to consume this mass flow.

3.2 Liquid Hydrogen Fuel Tanks

This part is the most critical part in the eye of the general population. Its design and location must not only satisfy technical expectations but also the desire for safety of the passengers, which are not always based on scientific parameters [22]. For the tank location several options are examined, but the location behind the rear bulkhead shows to be the best because of the following reasons:

3 Aircraft Components

- no external body needed
- the cabin is undisturbed
- the area is empty nevertheless
- the chimney for refueling can be placed conveniently close inside the vertical tail
- the flow of the hydrogen fuel from the tank through the components to the fuel cell is optimized regarding length

In the automotive industry the hydrogen is stored in a gaseous state because it is easier to store for a longer time, which is necessary for the way cars are used [23]. The downsides are the lower volumetric density and the high pressures the tank must endure. Storing the hydrogen in its cryogenic state achieves the highest volumetric density for hydrogen at 8 MJ/L [24].

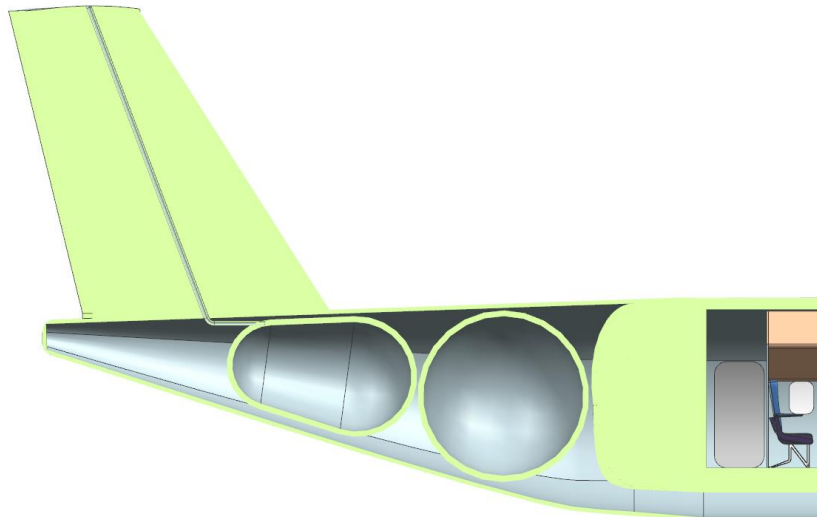


Figure 3-1: Shape and location of LH₂ tanks

For the construction of the tanks, the shape and the insulation thickness influence the amount of boil-off happening during the flight, resulting in loss of energy available to cool the components [25]. To accommodate the required fuel amount of the mission and satisfy the requirements in CS-25.953 [26], a conical tank and a bigger cylindrical tank are used. The wall thickness regarding strength and insulation increases for the conical tank but enables a more space efficient use of the tail section. The wall thickness was derived from Silberhorn et al. [25] for a tank located in the rear of the aircraft, the exact number being 70 mm. The fuel containment mass for the investigated aircraft is 36 % of the contained fuel mass [25]. This factor was increased to 40 % for HAIQU since the smaller and less cylindrical shapes of the tanks will result in higher loads for the tank, requiring more mass.

3.3 Battery

To define the battery, six important parameters were considered: Specific Energy, Specific Power, Cost, Life Span, Safety and Performance. Lithium-ion batteries currently dominate the automotive and aviation industries. The three most promising concepts for future batteries are Lithium Cobalt Oxide (LiCoO_2) – LCO, Lithium Nickel Manganese Cobalt Oxide (LiNiMnCoO_2) – NMC, and Lithium Iron Phosphate (LiFePO_4) – LFP batteries [27]. Each of those compositions has its own characteristics, with some being more developed than others [28]. A comparison can be seen in Figure 3-2.

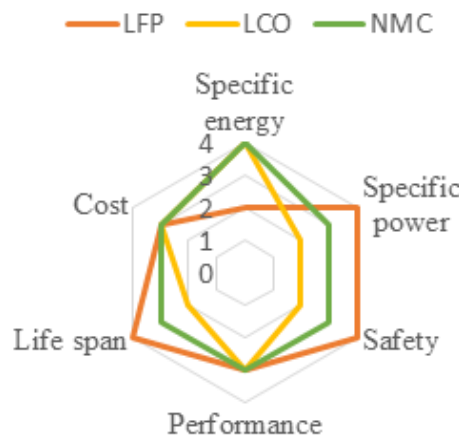


Figure 3-2: Snapshot of LFP, LCO and NMC batteries comparison [28]

However, the batteries can be adapted to suit the application specific need for power- and energy-density. Since the battery is only used to cover peak power needs and provide emergency power in case of a fuel cell failure, the focus lies on the specific power value and battery charge and discharge rates. A graph correlating specific power and specific energy is shown in Figure 3-3 [29].

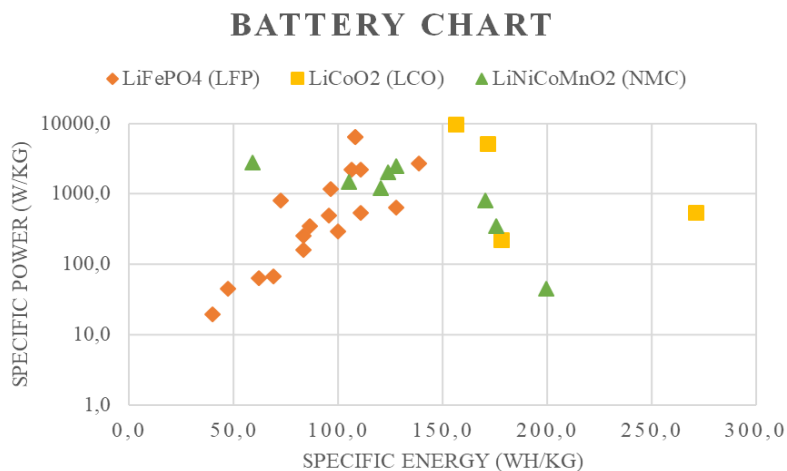


Figure 3-3: Specific power vs. specific energy of Li-Ion batteries distinguished by cell chemistry [29]

3 Aircraft Components

Although more criteria can be taken into account to choose the battery, the three main requirements were the Specific Power, C-Rate and the Safety of the technology used. Safety plays an important role because lithium batteries represent a risk factor due to the fact that the existing cargo fire suppression compartment has rates that are not as effective in mitigating the fire produced by these batteries [30]. Since batteries of this size and capacity will be newly introduced to the aviation sector, security will allow users to provide greater reliability of consumption. Moreover, LFP Lithium-ion batteries normally charge at a lower rate, often up to 1.5 C rate and the LFP chemistries' useful life can range between 3,000 to 5,000 cycles [31]. Given the high specific powers that the LFP batteries can reach and that they have already been introduced to the market [32], it was chosen as the battery composition for HAIQU.

The performance of the selected group of lithium batteries is shown Figure 3-3. From the data, the optimal values for HAIQU to cover the requirements of propulsion are 140 Wh/kg for energy density and 2000 W/kg for specific power on the cell level.

3.4 Electric Motor

The feasibility of a 1 MW electric motor with the power density of >13 kW/kg was investigated in [33]. This is four times higher than current state-of-the-art (SoA) electric motors [34]. The power density of HAIQUs electric motors is about 15 kW/kg and is estimated by [35]. Electric motors are well scalable and adjustable by the required power [36]. One HAIQU electric motor is designed for a shaft power of 900 kW at a weight of 64 kg.

High Temperature Superconductors (HTS) that will be operational in the Year 2030 have similar performance values to the HAIQU electric motors [37]. Based on the mass-equation for HTS $m_{HTS} = 2.28 * P^{0.6616}$ [36] the HAIQU electric motors are 5 % heavier

Furthermore, an electric motor efficiency of > 96 % is possible for HTS [33]. The efficiency of one HAIQU motor is estimated with 98 % [18].

3.5 Propeller

The use of electric energy as propulsion energy enables an almost free positioning of the propellers and motors. The current trends are the use of WTP, boundary layer ingestion (BLI) and distributed electric propulsion (DEP). Considering those concepts individually, WTP promises an improvement of up to 50 % less induced drag during climb and 25 % less during cruise [38] on a wing level and up to 15 % less total drag on aircraft level [39]. Blaesser et al. [40] have investigated the power distribution of an ATR 42-500 with WTP and conventional propellers. A power split of 50-50 between the WTP and the inbound propellers was identified to be the optimum, as the split reduces the disc loading and therefore reduces the total required power

3 Aircraft Components

by 5 % compared to a configuration with one propulsor per wing. While the induced drag is reduced when using only one engine per wing, the effects of the disc loading are dominating in comparison to the relatively small impact of the additional induced drag by the propellers. A secondary effect is a decrease of the wingtip vortex intensity through the WTP [38] which leads to a significant noise reduction [41].

Research regarding BLI showed that the positive effect increased with speed, making the use at the relative low speed of HAIQU less suitable. DEP showed promising results in an isolated setting, but further analysis on aircraft level showed no effect or even negative effects for this application [42].

Sizing investigations made clear, that the vertical tailplane makes only a small contribution into the compensation of a yaw moment when using WTP. Much more the available power of the wingtip propeller has a significant influence onto the yaw stability. Further, the yaw stability will be reconsidered in the following empennage section. Regarding the required climb angle during takeoff, an equally distributed power loading is preferred in case of a potential engine failure to provide the optimal power independently of the position of the failing engine.

From the mentioned boundary conditions, the power split of HAIQU is set to a 50-50 power split between WTP and the conventional propellers during take-off.

3.6 Fuselage

The fuselage follows a conventional basic design but employs a secondary, non-pressurized hull below the pressurized cabin section. The lower section is used for the propulsion components, TMS, and the gear. This is shown in Figure 3-4.

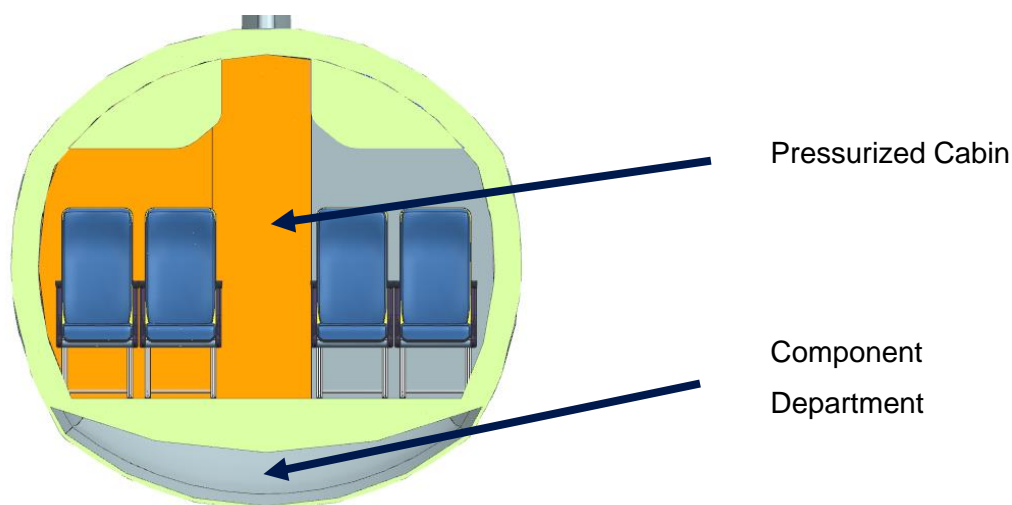


Figure 3-4: Cross-section of HAIQU showcasing the two sections. The lower section in grey houses the TMS, electronics and the gear while the upper section houses the cabin

3 Aircraft Components

The length has increased by 14 % to accommodate the fuel tank [3]. The fuselage is made of 50 % FRP saving 15 % on the mass compared to the reference aircraft. The seating configuration is single aisle with 4 seats abreast, with one row featuring just two seats to accommodate the last two seats.

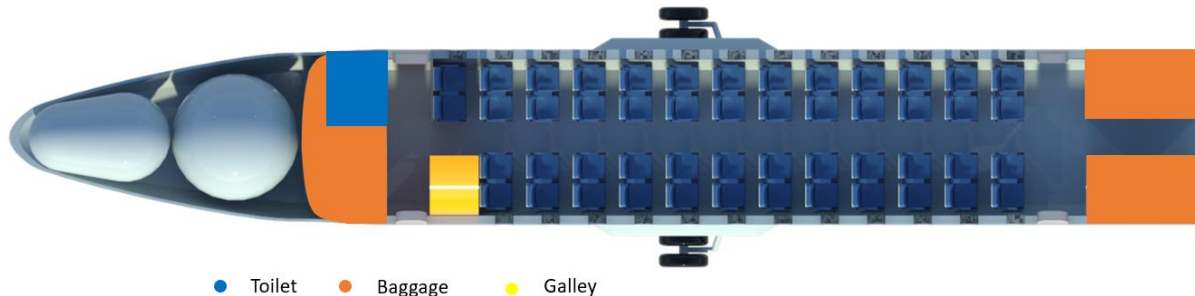


Figure 3-5: Cabin Layout of HAIQU

The conventional design has been proven successful and demands no further development costs, saving on the development cost. The baggage is stowed behind the rear galley, being accessed through a door inside the cabin, as well as in the front of the aircraft, with the door on the outside. The cockpit is a SoA digital glass cockpit with a very similar layout to the ATR to reduce pilot training costs. The layout can be seen in Figure 3-5.

3.7 Wing

For the wing design the classical configuration of high wing and T-tail is chosen [43]. It offers the best compromise for regional aircraft and other configurations bring no significant benefit in combination with hybrid electric propulsion compared to it.

The shape of the main wing is a two-shape design, with a rectangular shape from the centerline towards the inboard motor and a trapezoid shape from there until the outboard motor. The wing features single segment fowler flaps [44] that stretch for 60 % of the span with a depth of 17 %.

As wing profile the proven parameters of the reference aircraft were selected leading to a NACA 43018 at the root and a NACA 43013 at the tip [45]. With the aerodynamic coefficients from these profiles, the coefficients of the wing can be derived using Raymer sizing methods [43].

Additionally, the concept of laminar-flow profiles [46] was investigated in a trade-off study but in the following discarded based on the too high Reynolds number in the regional aviation sector and the short laminar areas due to the implementation of four propellers.

A trade-off study was done regarding the wingspan of the aircraft. This resulted in an improvement of the total aircraft with increasing wingspan with equal wing loading and power loading.

3 Aircraft Components

With the wingspan increasing 16 % from 24.6 m of the reference aircraft to 28.5 m while having similar wing areas the aspect ratio also increases. This in turn reduces the induced drag, resulting in the improvement of the aircrafts performance.

Contrary to current generation aircraft the wing is not used to store fuel and is therefore not subjected to passive stress relieve. The advantage of the WTP is the mass of the motor, gearbox, DC/AC converter and propeller acting as load reducing bending moment with a long lever arm. This results in an increase of 6 % in wing root bending moment compared to 16 % more without the WTP at MTOM and an increase of 9 % compared to 19 % with empty tanks. The additional stress is compensated by applying a factor of 6 % to the wing mass, since the maximum absolute bending moment occurs at MTOM. With increased wingspan the additional wing root bending moment is also decreased, further improving the aircrafts performance by reducing weight.

3.8 Empennage

The T-shaped empennage was chosen to reduce the wing- and propeller-wake interaction with the tail plane. Furthermore, the volume coefficient of the vertical tail area V_h is set to a larger value than the reference aircraft to provide enough yawing moment during wingtip engine-failure. This larger volume coefficient was calibrated on the reference aircraft to provide the same yawing potential. This was done because the reference values of the volume coefficient are derived from non-WTP configurations, resulting in lower than required volumes.

3.9 Landing Gear

The landing gear is integrated in the body, similar to the ATR family and Airbus A400M [47]. The second option is to integrate the main landing gear into the wing or cowling, as on the Dash 8 [48]. Due to the large distance between wing and ground and the non-existent cowling, a very long and massive landing gear would have to be designed. The clearance between the outer propellers and the ground is enough to satisfy the ground clearance requirements, to protect the propeller during gusty landings a retractable wheeled strut was integrated at the tip to protect the propeller if the available clearance is not sufficient. The main landing gear has two wheels each, the same goes for the steerable nose landing gear.

3.10 Electric Green Taxiing System

As part of HAIQU's energy saving and noise reduction strategy, an electric green taxiing system (EGTS) is deployed. With the use of the battery as the energy storage system (ESS) and the PEMFC as energy source, the integrated electric traction drive system (ETDS) in the nose

4 Performance and Technical Data

landing gear enables the full movement of the aircraft during the taxiing phase without giving thrust over propeller drive [49].

In general, the aircraft taxiing phase takes between 10 to 30 % of total flight time in Europe [50] which equals to 10 % of total fuel consumption in comparison to a regular aircraft [51]. In combination with a hybrid powertrain like HAIQU's, the EGTS could further reduce the fuel consumption e.g., due to the omission of the auxiliary power unit [52]. With regenerative braking during the taxiing phase, 15 % of the energy could be recovered [49] and the lifetime of the brake system would be increased [53]. The utilized EGTS dimensions are calculated with the formulas from Heinrich et al. [54] and they are shown together with the Technology Readiness Level (TRL) in Table 3-2.

Power required	68 KW
Mass EGTS	123 kg
Max Taxiing Speed	23 km/h
TRL of all components [55]	6 or higher

Table 3-2: EGTS-dimensions and TRL

The most important advantages are improvement of push back time and elimination of the push back support for reverse taxiing [54]. The more autonomous operations improve traffic flows and flight punctuality [53]. Furthermore, the safety for the airport ground crews is increased [55].

4 Performance and Technical Data

The following chapter discusses the impact of hybrid technology on the flight and ground performance of HAIQU and the resulting design differences to the reference aircraft.

4.1 Payload-Range diagram

One major issue arose with regards to the payload-range diagram and the TLARs: If the design point was met, it was impossible to achieve any range with the full payload (See red line and diamond in Figure 4-1). This is the case because the hydrogen fuel mass for the design mission in the first design phase was about 400 kg while the difference between design payload and maximum payload is 500 kg. This results in an aircraft being 100 kg heavier than the MTOM without carrying fuel. The battery that is still able to carry energy, since its mass does not change when charged, does not have sufficient energy storage to perform a flight with reserve in any case. Increasing the battery size does not solve this issue either since the hydrogen fuel

4 Performance and Technical Data

mass is decreasing with this measure, resulting in an even more overloaded aircraft at maximum payload. To solve this issue two possibilities are available:

- Decrease the fuel efficiency to increase the required fuel for the design mission to more than 500kg, or
- Change the design point to achieve a useable range at maximum payload while still being able to fulfill the requirements of the original design point

Since decreasing the fuel efficiency of the aircraft would defy all logic, common sense and fail the goal of aircraft design, the design point is adjusted to achieve a usable Payload-Range-Diagram. In Figure 4-1 the two different payload-range diagrams are depicted, showing that the old design point in red results in the failing of one of the TLARs. The old design point is still achievable with the new interpretation of the design point.

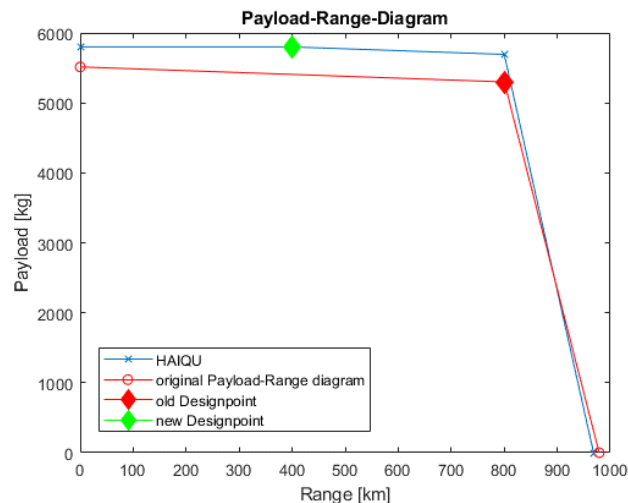


Figure 4-1: Payload-Range-Diagram comparison

The Payload-Range-Diagram consist of three separate lines. The first line, a horizontal one shows the limit of the payload regarding the maximum zero fuel mass (MZFM). This line performs in the same way for hydrogen aircraft as for conventional aircraft. The second line in the middle, showing a shallow decline, is limited by the MTOM. Along this line payload is exchanged with fuel to achieve a higher range. This line is usually angled between 30° and 60° downward for conventional aircraft. For HAIQU it is very shallow at below 10°. This is attributed to the high gravimetric density of LH₂ (120 MJ/kg [56]) compared to Jet-A1 (42.8 MJ/kg [57]) with a factor of 2.8. Furthermore, the efficiency of the chemical powerplants for each fuel type (PEMFC and gas turbine) vary, with the PEMFC having a higher efficiency of 53 % [18] compared to 30 % [58] for the PW127 turboshaft gas turbine in cruise condition. The third line, steep declining on the right is limited by the fuel tank size. To increase the range in this area, payload is removed until the aircraft is empty. This line is steeper than for most conventional aircraft, since the design mission range is very low compared to similar aircraft. The reserves

4 Performance and Technical Data

as well as the fuel masses required for takeoff, climbing and descending contribute to more than 30 % of the total tank volume, limiting the ferry distance significantly.

4.2 Performance Characteristics

To validate the fulfillment of the TLARs, the performance characteristics of HAIQU are calculated. The main characteristics are presented in Table 4-1: Main performance characteristics of HAIQU while a more detailed tabular technical summary can be found in Appendix B.

Table 4-1: Main performance characteristics of HAIQU

Aircraft Performance	Achieved Characteristic
Take-off distance at MTOM, ISA, SL	980 m
Landing distance at MLM, ISA, SL	775 m
Maximum rate of climb at MTOM, ISA, SL	2400 ft/min
Cruise speed, Mach, and Altitude	298 kt/0.48 Ma @ FL170
L/D in cruise	12.9
LH ₂ consumption in cruise	2.2 kg/min
Total Energy consumption for DOC mission	2360 kWh
Energy consumption by mission segment	Taxi 0.01, T/O 0.02, CLB 0.12, CRZ 0.42, DES 0.02, APP 0.01, CLB_res 0.09, CRZ_res 0.30, DES_res 0.02, APP_res 0.01

4.3 Mass Estimation

Most of the individual component masses are calculated by semi-empirical equations, which were derived by Torenbeek [59]. First assumptions to start the iterative equations are made with existing data of the reference aircraft [17]. The masses of the fuel cell and batteries are calculated using the data provided by Hartmann et al. [18] as well as applying the power density of the selected battery composition to the required power. Since the power density was given at cell level, an estimate for the pack was made by using an estimation method described by Berseneff [60].

4 Performance and Technical Data

Component	Mass [kg]	Component	Mass [kg]
Wing	900	Flight Systems	2590
Fuselage	1950	Fuel cell	2780
Empennage	320	Battery	1950
Landing Gear	620	Crew & Equipment	1050
Control mechanism	205	Miscellaneous	150
Electric motors	255	Gearboxes	140
EGTS	120	Cowling	170

Table 4-2: Mass of components

Designation	Mass [kg]
Operating Mass Empty	13200
Fuel + Reserve	300
Max. Payload	5800
Max. Take-off Mass	19300

Table 4-3: Mass estimation for new Design Mission (400km @ 5800 kg)

Regarding lightweight construction, HAIQU has a composite vs. total structure volume ratio of 54 % leading to four times higher [44] usage of composite material in comparison with the reference aircraft. Fuhrer, the mean aerodynamic chord (MAC) is located at 23,8 % leading to a location of the center of gravity (CoG) at 11,35 m related to the defined coordinate system (origin 1m in front of the nose of the plane) at operating mass empty (OME). Considering the aircraft at OME without crew & PAX and with added max fuel mass, the maximum static margin is 33 % MAC.

4.4 Turnaround Process

The turnaround process is critical to the competitiveness of an aircraft. There are three significant differences between the current generation of regional aircraft and HAIQU: the refueling is not done at the wings, includes liquid hydrogen instead of jet fuel and the battery must be recharged too. The process is depicted in Figure 4-2 and each path is explained in chapter 4.4.1.

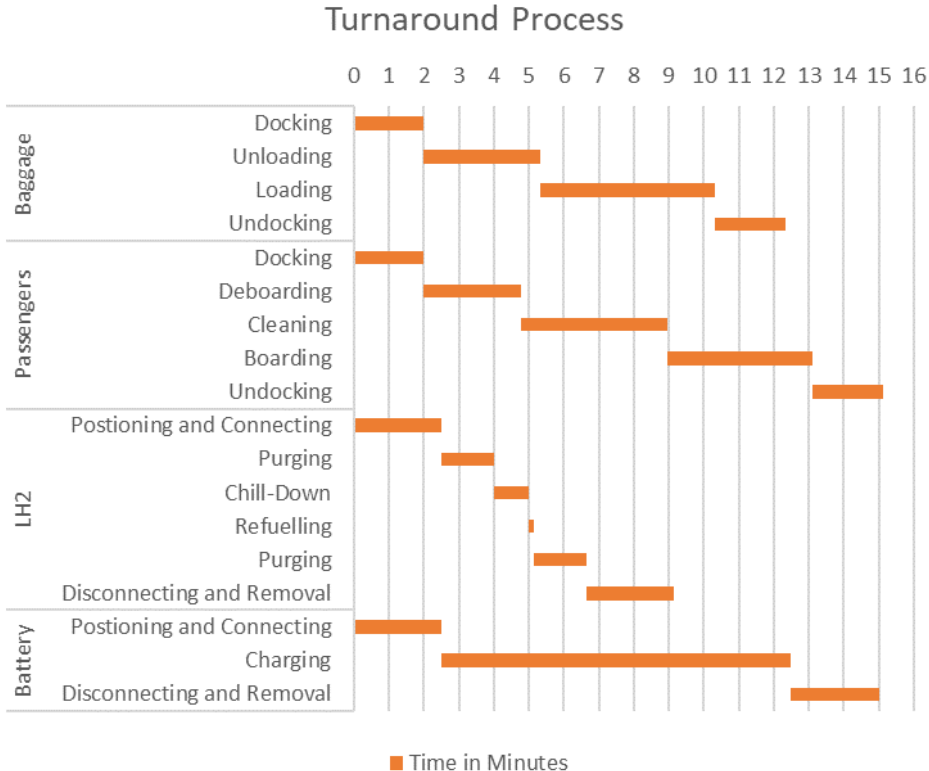


Figure 4-2: Gantt-Chart of the Turnaround Process

4.4.1 Aircraft Related Turnaround Characteristics

The repositioning of the refueling vehicles can interfere with passenger loading and unloading as well as the baggage loading and unloading. The refueling port at the aircraft is positioned as far rearward as possible, to keep the space next to the rear cabin doors free for baggage and passenger transfer. For safety reasons the refueling port must be far back, to increase the distance between the charge port for the battery and the possible exit of hydrogen from either the aircraft or the refueling vehicle.

As mentioned in Mangold et al. [61], the turnaround procedure regarding safety does not have to change for passengers or aircraft workers doing other jobs. The refueling process must be semi-automated or fully automated because of the increased weight of the hose. The total refueling time consists of six segments, each with a fixed length except for the refueling itself. The refueling time can be calculated by dividing the fuel mass of 420 kg by the mass flow of 20 kg/s [61] with to achieve a time of 21 s. In total, the refueling process according to the procedures of Mangold et al. [61] takes 10min for full refueling.

The battery charging is a critical time path for the turnaround because it is essential to be at the required state of charge (SOC) to perform the takeoff and serve as safety backup. Fully

4 Performance and Technical Data

charging the battery with a small 200 kW charger results in a C-Rate of 0.98C and a charging time of 62 min, surpassing the times of the other areas of the turnaround by 4 times. To reduce this time, the battery, being used only during takeoff and to mitigate the slow reacting nature of the fuel cell, will be charged in flight in the following scenarios:

- every time the throttle setting is decreased, and the fuel cell needs time to react
- during descent to keep the fuel cell running for component cooling
- during taxi to and from the runway, because the fuel cell provides more energy than the EGTS needs

During descend the battery can be charged at a C-rate of up to 2, providing at least 32 % of the max. stored energy during a normal descend. In normal conditions the battery is used purely in the takeoff and initial climbing phase, using less energy than provided during descend. In this phase a maximum discharge rate of 2.1 C is achieved. This eliminates the need for charging at airports for normal mission profiles. Since the price of electricity per energy unit is lower than the price of hydrogen, it makes sense to limit the recharging of the battery to a given SOC to allow the use of charging on the ground during the turnaround if available, resulting in an increase of efficiency of the flight since the battery can reduce the load on the PEMFC, increasing its efficiency this way. The required SOC is dependent on the available charging infrastructure at the airport. The aircrafts battery has more capacity than needed for the design mission, but this is intended as backup to combat wear in the components as well as serve as emergency backup. In normal operation the full capacity of the battery is not unlocked.

For the baggage unloading and loading the values for loading and unloading rate as well as the un-/docking times were taken from a Boeing 737-900 [62] since it also uses bulk cargo. This results in a total time of 12.3 min.

To calculate the time for passenger exchange and cleaning the passenger moving rates of 18 pax/min exiting and 12 pax/min entering per Type I door according to Airbus [63] and the cleaning rate of 3 seats/min per cleaner according to Fuchte [64] are used. The number of cleaners is dependent on the money the airline is willing to spend, but Fuchte [64] estimates four cleaners for an A320 and six cleaners for long range aircraft. If this was reduced to two cleaners for HAIQU because of the small size of the airplane, the turnaround would take 19.3 min since the passengers are the critical path. Increasing the number of cleaners decreases the time to 15.1 min. It must be said that this is quiet conservative, since the amount of dirt and waste produced by the passengers is much lower for a regional aircraft than a short-range aircraft simply because of the lack of catering and the shorter flight duration. Therefore, the number of cleaners is chosen to be four.

4.4.2 Airport Related Turnaround Characteristics

For an airport to be suitable to service flights from HAIQU aircraft two changes must be made to the current standard airport equipment:

- Storage and distribution equipment for liquid hydrogen
- Charging facilities to recharge the batteries

The hydrogen will be stored in tanks, preferably located close to the ramp to reduce the travel distance and therefore the losses [65]. It can be transferred using self-sufficient fuel trucks or by using a smaller truck supplying the equipment but connecting to an underground pipeline network of liquid hydrogen [61]. The truck variant is depending on the airports size, with the self-sufficient truck setup being more economical at airports consuming less than 125.000 t of LH₂ [66]. Since the job of a regional aircraft is often to transport passengers between small airports and large airports, they will encounter both types of refueling equipment.

Regarding the charging of the batteries, the likely charging supply powers are between 200 kW and 1000 kW. This results in a wide spread between the charging times for the aircraft. The option of introducing battery swapping to HAIQU was also considered, but since the aircraft will be operating in mostly smaller airports, the ground equipment cost for the airport combined with the additional working force to swap a battery would outweigh the benefit of faster replenishing the energy storage. This only applies to the small capacity of HAIQU, the approach can be different for aircraft with higher capacity batteries.

4.5 Sustainability

Assuming that the hydrogen (H₂) is produced in the today most common way as “grey” hydrogen, 9.3 kg of CO₂ per kg H₂ are emitted with current production technologies [67]. With a fuel burn of 172 kg H₂ for a flight range of 400 km, 3.7 t of CO₂ are emitted, leading to a CO₂ increase of 1,6 % in comparison to the reference aircraft.

However, hypothesizing an emission neutral H₂ production method (e.g., blue, green, or pink hydrogen) emitting 0 kg of CO₂ per kg H₂, 3,4 t of CO₂ can be saved per 400 km in comparison to the reference aircraft [2].

Furthermore, it must be pointed out, that the dumping of leftover liquid water resulting from the fuel-cell combustion has no significant greenhouse effect in the maximum operating altitude of 25,000 ft [68].

5 Direct Operating Costs

The Direct Operating Costs (DOC) must be calculated slightly differently to a conventional aircraft since there are two types of energy sources. Furthermore, the costs for noise and emissions vary a lot between the conventional, CO₂ emitting aircraft and HAIQU.

5.1 Assumptions

Different assumptions were made during the total cost calculation process. For the calculation of the depreciation, it was necessary to estimate a value of the service time of the aircraft, this service time was approximately 14 years. At the same time, it is necessary to define the inflation costs, which must be taken into account from the formulation of the AEA Method 1989 to the present, for this reason, a projected interest cost was introduced from 1989 to 2035. [69] This could generate an overestimation of the value given the age of the method. For fuel costs, the price is fluctuating considerably due to geopolitical disputes. The price of LH₂ at the beginning of the project was three times lower than the current price. The price used for the calculation is the result of a recent study and the value was taken for Europe in 2035 [70]. Given the age of the method, the costs for fees and charges did not conceive the new regulations of the 2000s for noise and pollution, for this reason additional costs for CO₂ and NO_x emissions were charged to the reference aircraft following the methodology of Johanning and Scholz [71].

Finally, it was necessary to adjust the payload and the mission range of the reference vehicle to the competition conditions since the adjusted values for the DOC are generally presented based on their design margins.

5.2 Resulting Cost for Design Mission

The method takes into account the costs of depreciation, interest, insurance, fuel, maintenance (Airframe and power plant), crew (Cabin and Cockpit) and fees and charges (Landing Fees, Navigation Charges, Ground Handling). Fees and Charges values may vary according to landing costs from one airport to another. In recent years some airports have introduced a release of Landing Fees if the plane is electric or hybrid, so it was necessary to introduce this consideration. A graph with the monetary values distributed in each of the sections of the DOC is shown below. The unit EUR/100S•km represents the costs in Euros per seat in 100 kilometers.

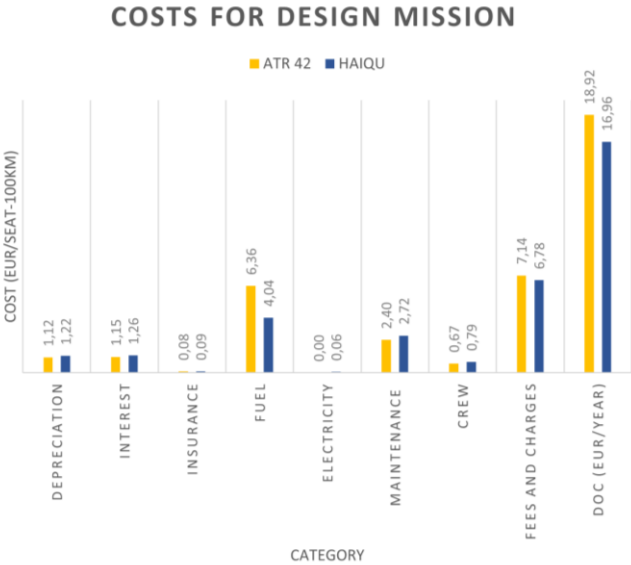


Figure 5-1: Cost for Design Mission for HAIQU based in 1509 flights per year

5.3 Resulting Cost for Benchmark Mission

A comparison with equal range and equal payload was used to obtain a true cost comparison with the reference aircraft. Additionally to the AEA methodology, costs for pollution and noise were added to the category of Fees and Charges, specifically in Ground Handling. A graph with this comparison is shown in Figure 5-2.

The new values for Fees and Charge related to Pollution and Noise are equivalent according to the equation for the AEA Method to 0.2 % and 0.02 % respectively of the total DOC [71] [72] [73]. Additionally, the prices of JET A-1 were estimated based on the development of the price of fossil fuels for the year 2035, which show a slight increase of 10 % of the current price [74].

Electricity prices, for their part, will remain at least constant given the continent's energy transformation [75]. For 2035 a price reduction for hydrogen between EUR 1.3 and EUR 2.6 per Kilogram is expected [76], which would imply a greater benefit from the use of a hybrid airplane.

6 Conclusion

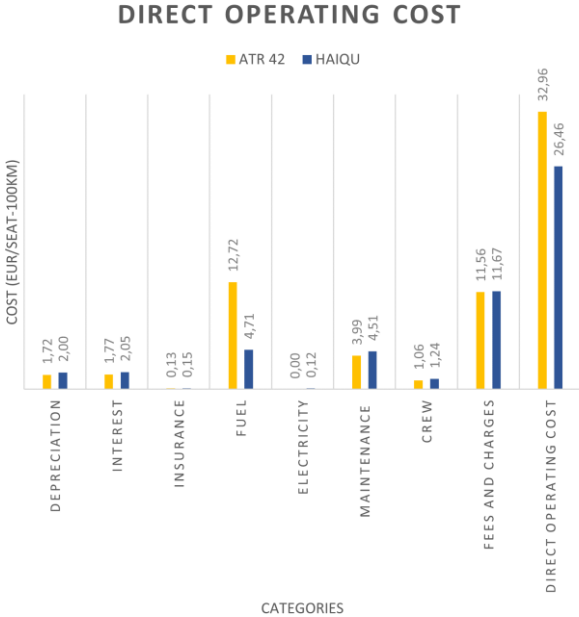


Figure 5-2: Direct operation cost from reference aircraft and HAIQU based in 1810 flights per year.

6 Conclusion

The HAIQU design proves the feasibility of a fuel cell powered hybrid-electric regional aircraft for 50 passengers and thus fulfills the challenge’s task. Much more this work goes further in not only presenting a hybrid aircraft but also an emission neutral aircraft, which leads the way to future sustainable aviation.

Keeping the forecast of fuel prices in mind, HAIQU simultaneously outlines a more cost-efficient operation in comparison to conventional regional aircraft.

Further, HAIQU presents an innovative design while guaranteeing a safe realizability for the year 2035. Thanks to many used synergies the applied new technologies can realize their maximum potential. HAIQU can replace current regional aircraft seamlessly regarding use, the only difference is the required new ground equipment regarding recharging and refueling.

Finally, we are certain that this concept can realistically enter service in 2035 and the fuel cell technology will revolutionize the future aircraft market as well as kickstart the new hydrogen aircraft generations.

References

- [1] FUTPRINT50, "futprint50.eu," 1 April 2022. [Online]. Available: <https://futprint50.eu/2nd-futprint-academy>.
- [2] ATR, "ATR-aircraft," June 2022. [Online]. Available: https://www.atr-aircraft.com/wp-content/uploads/2022/06/ATR_Fiche42-600-3.pdf. [Accessed 12 07 2022].
- [3] ATR-aircraft, "ATR Family," ATR, Blagnac cedex - France, 2014.
- [4] ATR, "ATR42-600S," 11 May 2022. [Online]. Available: https://www.atr-aircraft.com/wp-content/uploads/2022/06/ATR_Fiche42-600S-3.pdf. [Accessed 13 July 2022].
- [5] Verein Deutscher Ingenieure e.V., "Technisch-wirtschaftliche Bewertung – VDI 2225 Blatt 3," Beuth Verlag GmbH, Berlin, 1998.
- [6] "Modern Aero Engines: Multifuel vs. Hybrid vs. Electric," European Security and Defence, 12 January 2022. [Online]. Available: <https://eurosd.com/2022/01/articles/exclusive/24452/modern-aero-engines-multifuel-vs-hybrid-vs-electric/>. [Accessed 22 August 2022].
- [7] G. Willmer, "Green aviation takes wing with electric aircraft designs," European Commission, Brussels, 2022.
- [8] G. Palaia, D. Zanetti, K. A. Salem, B. Vincenzo and B. Cipolla, "THEA-CODE: A design tool for the conceptual design of hybrid-electric aircraft with conventional or unconventional airframe configurations," Mechanics and Industry, Pisa, 2021.
- [9] I. Geiß, "Sizing of the Series Hybrid-electric Propulsion System of General Aviation Aircraft," Stuttgart University, Stuttgart, 2020.
- [10] R. Winkler and R. Henke, "Zero Emission White Report," DLR, Stuttgart, 2020.
- [11] K. Saikia, B. Kakati, B. Boro and A. Verma, "Current Advances and Applications of Fuel Cell Technologies," Springer, Singapur, 2018.
- [12] S. K and H. E, "A Proton Exchange Membrane & Solid Oxide Fuel Cell comparison," Chalmers University of Technology, Gothenburg, 2019.
- [13] "Power-to-Weight-Ratio," Autopedia, 6 March 2019. [Online]. Available: https://automobile.fandom.com/wiki/Power-to-weight_ratio#Examples. [Accessed 22 August 2022].
- [14] J. Kallo, Interviewee, *Hydrogen - non drop-in fuel for aviation*. [Interview]. 22 June 2022.
- [15] J. McMicking, Interviewee, *Powering Clean Aviation*. [Interview]. 22 June 2022.
- [16] B. Law, Interviewee, *Hydrogen - non drop-in fuel for aviation*. [Interview]. 22 June 2022.
- [17] IHS Jane's, *Jane's All the World's Aircraft 2010-2011*, IHS Jane's, 2011.
- [18] C. Hartmann, J. K. Nøland, R. Nilssen and R. Møllerud, "Dual Use of Liquid Hydrogen in a Next-Generation PEMFC-Powered Regional Aircraft with Superconducting Propulsion," IEEE, 2022.

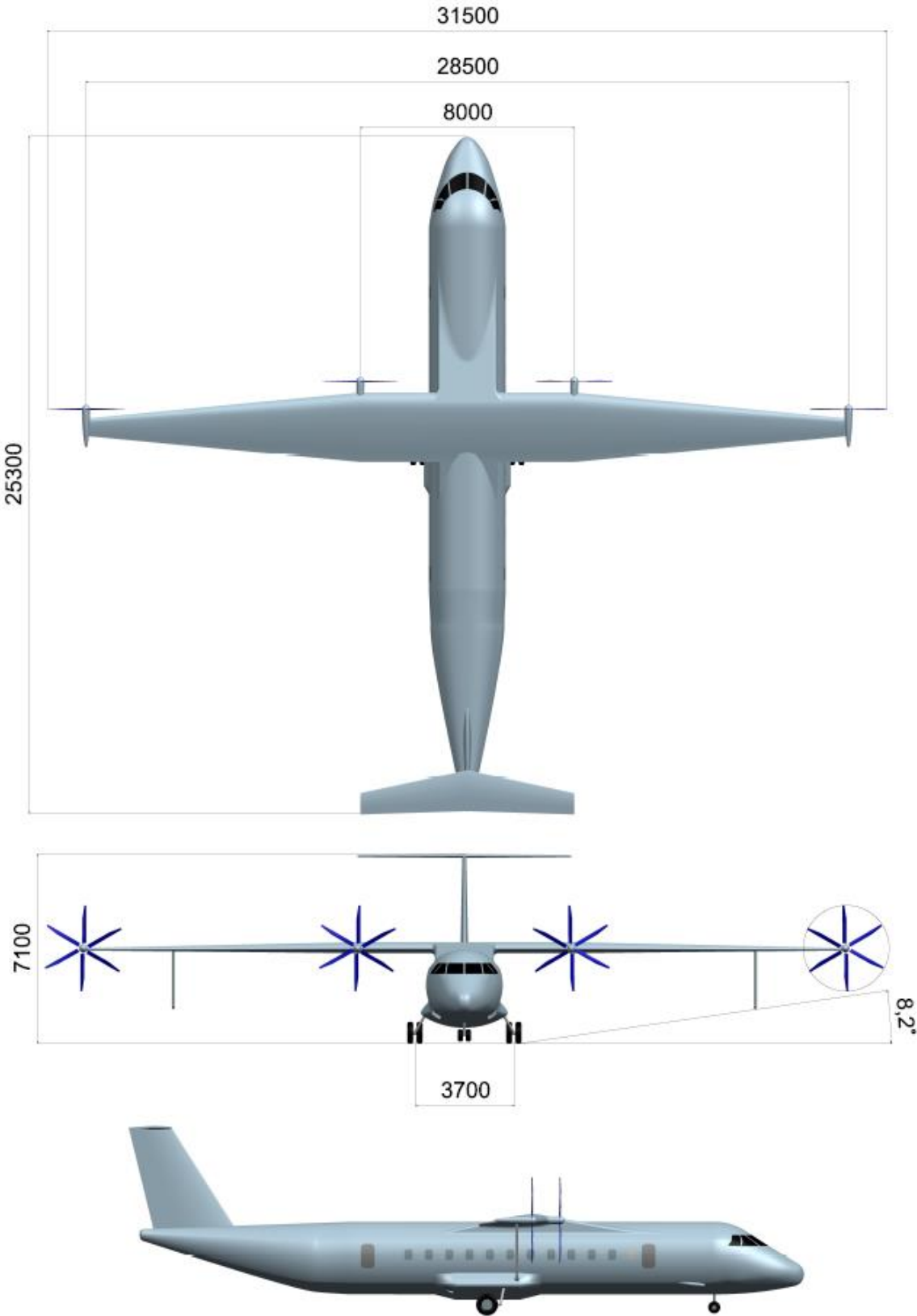
- [19] H. Kellermann, M. Lüdemann, M. Pohl, Hornung and Mirko, "Design and Optimization of Ram Air–Based Thermal Management Systems for Hybrid-Electric Aircraft," MDPI, 2020.
- [20] J. W. Chapman, S. L. Schnulo and M. P. Nitsche, "Development of a Thermal Management System for Electrified Aircraft," NASA, 2020.
- [21] L. Piancastelli, L. Frizziero and G. Donnici, "THE MEREDITH RAMJET: AN EFFICIENT WAY TO RECOVER THE HEAT WASTED IN PISTON ENGINE COOLING," ARPN, 2015.
- [22] K. Ono, E. Kato and K. Tsunemi, "Does risk information change the acceptance of hydrogen refueling stations in the general Japanese population?," International Journal of Hydrogen Energy, 2019.
- [23] E. Rivard, M. Trudeau and K. Zaghib, "Hydrogen Storage for Mobility: A Review," MDPI, 2019.
- [24] Department of Energy - USA, "Hydrogen Storage," [Online]. Available: <https://www.energy.gov/eere/fuelcells/hydrogen-storage>. [Accessed 14 August 2022].
- [25] D. Silberhorn, G. Atanasov, J.-N. Walther and T. Zill, "Assessment of Hydrogen Fuel Tank Integration at Aircraft Level," DLR, Darmstadt, 2019.
- [26] EASA, "Certification Specifications and Acceptable Means of Compliance for Large Aeroplanes (CS-25)," EASA, 2021.
- [27] G. Saldaña, J. Martín, I. Zamora, F. Asensio and O. Oñederra, "Analysis of the Current Electric Battery Models for Electric Vehicle Simulation," MDPI, Bilbao, Spain, 2019.
- [28] Batteryuniversity, "Batteryuniversity," 16 August 2022. [Online]. Available: <https://batteryuniversity.com/article/bu-205-types-of-lithium-ion>.
- [29] P. Stenzel, M. Baumann, J. Fleer, B. Zimmermann and M. Weil, "Database development and evaluation for techno-economic assessments of electrochemical energy storage systems," Researchgate, Dubrovnik, Croatia, 2014.
- [30] "Lithium Batteries Safe to Fly," Airbus, January 2016. [Online]. Available: <https://safetyfirst.airbus.com/lithium-batteries-safe-to-fly/>. [Accessed 22 August 2022].
- [31] V. Karimov, "New Tests Prove: LFP Lithium Batteries Live Longer than NMC," OneCharge, 30 March 2021. [Online]. Available: <https://www.onecharge.biz/es/sin-categorizar/lfp-lithium-batteries-live-longer-than-nmc/>. [Accessed 21 August 2022].
- [32] S. Kothari, "BYD Blade Battery," 16 08 2022. [Online]. Available: <https://topelectricsuv.com/news/byd/byd-blade-battery-update/>.
- [33] A. Yoon, X. Yi, J. Martin, Y. Chen and K. Haran, "Preliminary optimization efforts and loss analysis suggests a 1 MW machine with power density of > 13kW/kg and efficiency of > 96% is achievable," 28 April 2016. [Online]. Available: <https://ieeexplore.ieee.org/abstract/document/7459221>. [Accessed 5 July 2022].
- [34] M. D. Hathaway, R. D. Rosario and N. K. Madavan, "NTRS - NASA Technical Reports Server," 16 June 2014. [Online]. Available: <https://ntrs.nasa.gov/citations/20140008324>. [Accessed 28 June 2022].

- [35] M. Komiya, T. Aikawa, H. Sasa and S. Miura, "Design Study of 10 MW REBCO Fully Superconducting Synchronous Generator for Electric Aircraft," IEE, 2019.
- [36] T. Lukaczyk, A. D. Wendorff, E. Botero, T. MacDonald, T. Momose, A. Variyar, J. M. Vegh, M. Colonno, T. D. Economon, J. J. Alonso, T. H. Orra and C. R. Ilario da Silva, "SUAVE: An Open-Source Environment for Multi-Fidelity Conceptual Vehicle Design," July 2015. [Online]. Available: https://www.researchgate.net/publication/282253546_SUAVE_An_Open-Source_Environment_for_Multi-Fidelity_Conceptual_Vehicle_Design. [Accessed 4 July 2022].
- [37] C. A. Luongo, P. J. Masson, T. Nam, D. Mavris, H. D. Kim, G. V. Brown, M. Waters and D. Hall, "Next Generation More-Electric Aircraft:," *IEEE Transactions on Applied Superconductivity*, Vols. No. 3, Part 2, no. 19, pp. 1055-1068, 2009.
- [38] T. Sinnige, N. v. Arnhem, T. C. A. Stokkermans, G. Eitelberg and L. L. M. Veldhuis, "Wingtip-Mounted Propellers: Aerodynamic Analysis of Interaction Effects and Comparison with Conventional Layout," *Journal of Aircraft*, vol. 56, no. 1, 2019.
- [39] O. Pfeifle, S. Notter, W. Fichter, D. P. Bergmann, J. Denzel and A. Strohmayr, "Verifying the Effect of Wingtip Propellers on Drag through In-Flight Measurements," University of Stuttgart, Stuttgart.
- [40] N. J. Blaesser, Propeller-Wing Integration on the Parallel Electric-Gas Architecture with Synergistic Utilization Scheme (PEGASUS) Aircraft, 978-1-62410-578-4 ed., vol. AIAA Scitech 2019 Forum, San Diego, California: American Institute of Aeronautics and Astronautics, 2019.
- [41] E. Schneehagen, T. Geyer and E. Sarradj, "Aeroacoustic noise reduction by application of end plates on wall-mounted finite airfoils," *Experiments in Fluids*, vol. 62, no. 1, 24 April 2021.
- [42] R. de Vries, M. Brown and R. Vos, "Preliminary Sizing Method for Hybrid-Electric Distributed-Propulsion Aircraft," Delft University of Technology, Delft, 2019.
- [43] D. P. Raymer, Aircraft Design: A Conceptual Approach (AIAA Education Series), Transatlantic Publishers, 2012.
- [44] A. v. Croy, "Airwork," 2007. [Online]. Available: https://airwork.biz/wp-content/uploads/2009/03/atr_e1.pdf. [Accessed 2 June 2022].
- [45] M. F. Niță, "Aircraft Design Studies Based on the ATR 72," Department of Automotive and Aeronautical Engineering, HAW Hamburg, 2008.
- [46] M. S. Selig, M. D. Maughmer and D. M. Somers, "Natural-laminar-flow airfoil for general-aviation applications," *Journal of Aircraft*, vol. 32, no. 1, July 1995.
- [47] Safran Group, "safran-group," Safran, [Online]. Available: <https://www.safran-group.com/products-services/nose-and-main-landing-gears-most-advanced-military-transport-aircraft-21st-century>. [Accessed 10 08 2022].
- [48] Bombardier, "Smartcockpit," [Online]. Available: https://www.smartcockpit.com/docs/Q400-Landing_Gear_1.pdf. [Accessed 12 08 2022].
- [49] M. T. E. Heinrich, F. Kelch, P. Magne and A. Emadi, "Regenerative Braking Capability Analysis of an Electric Taxiing System for a Single Aisle Midsize Aircraft," *IEEE Transactions on Transportation Electrification Bd. 1*, pp. 298-307, October 2015.

- [50] I. Deonandan and H. Balakrishnan, "Evaluation of Strategies for Reducing Taxi-out Emissions at Airports," 2010. [Online]. Available: <http://arc.aiaa.org/doi/abs/10.2514/6.2010-9370>. [Accessed May 2022].
- [51] Y. Nicolas, "eTaxi - Taxiing aircraft with engines stopped," *Airbus FAST magazine*, no. 51, pp. 2-10, 2013.
- [52] C. L. Pastra, C. Dull, R. Berumen, C. Yumuk, G. Cinar and D. N. Mavris, "Viability Study of an Electrified Regional Turboprop," in *2022 IEEE/AIAA Transportation Electrification Conference and Electric Aircraft Technologies Symposium (ITEC+EATS)*, Anaheim, CA, USA, 2022.
- [53] H. Cheaito, B. Allard and G. Clerc, "Proof of concept of 35 kW electrical taxiing system in more electrical aircraft for energy saving," *International Journal of Electrical Power & Energy Systems*, vol. 130, September 2021.
- [54] M. T. E. Heinrich, F. Kelch, P. Magne and A. Emadi, "Investigation of regenerative braking on the energy consumption of an electric taxiing system for a single aisle midsize aircraft," in *IECON 2014 - 40th Annual Conference of the IEEE Industrial Electronics Society*, Dallas, TX, USA, 2014.
- [55] M. Lukic, P. Giangrande, A. Hebala, S. Nuzzo and M. Galea, "Review, Challenges, and Future Developments of Electric Taxiing Systems," *IEEE Transactions on Transportation Electrification*, vol. 5, no. 4, pp. 1441-1457, December 2019.
- [56] Office of Energy Efficiency & Renewable Energy, "Hydrogen Storage," [Online]. Available: <https://www.energy.gov/eere/fuelcells/hydrogen-storage>. [Accessed 20 August 2022].
- [57] The Physics Factbook, "Energy Density of Aviation Fuel," [Online]. Available: <https://hypertextbook.com/facts/2003/EvelynGofman.shtml>. [Accessed 20 August 2022].
- [58] SCRIBD, "PW127 Turboprop Sales Specification No 1009 Datasheet," [Online]. Available: <https://de.scribd.com/document/330696372/PW127-Turboprop-Sales-Specification-No-1009-Datasheet>. [Accessed 20 August 2022].
- [59] E. Torenbeek, *Advanced aircraft design: conceptual design, analysis, and optimization of subsonic civil airplanes*, Chichester, West Sussex, United Kingdom: John Wiley & Sons Inc, 2013.
- [60] B. Berseneff, "An introduction to energy storage for aircraft applications," 2022.
- [61] J. Mangold, D. Silberhorn, N. Moebis, N. Dzikus, J. Hoelzen, T. Zill and A. Strohmayer, "Refueling of LH2 Aircraft—Assessment of Turnaround Procedures and Aircraft Design Implication," 2022. [Online]. Available: <https://doi.org/10.3390/en15072475>. [Accessed 10 July 2022].
- [62] Boeing, "737 - Airplane Characteristics for Airport Planning," 2005.
- [63] AIRBUS, "AIRCRAFT CHARACTERISTICS - AIRPORT AND MAINTENANCE PLANNING," Airbus, Blagnac Cedex, 2020.
- [64] J. C. Fuchte, "Enhancement of Aircraft Cabin Design Guidelines with Special Consideration of Aircraft Turnaround and Short Range Operations," *Technischen Universität Hamburg-Harburg*, Hamburg, 2014.

- [65] M. Marksel, A. B. Prapotnik, R. Kamnik, K. Hanzic, T. Letnik and S. Bozicnik, "ADAPTATION OF AIRPORT INFRASTRUCTURE FOR OPERATION OF ICE-HYBRID AND FUEL-CELL AIRCRAFT," MAHEPA, 2020.
- [66] J. Hoelzen, M. Flohr, D. Silberhorn, J. Mangold, A.-. Bensmann and R. Hanke-Rauschenbach, "H2-powered aviation at airports – Design and economics of LH2 refueling systems," May 2022. [Online]. Available: <https://www.sciencedirect.com/science/article/pii/S2590174522000290#!>. [Accessed 15 August 2022].
- [67] R. Rapier, "Forbes," 6 June 2020. [Online]. Available: <https://www.forbes.com/sites/rrapier/2020/06/06/estimating-the-carbon-footprint-of-hydrogen-production>.
- [68] B. Kärcher, "Formation and radiative forcing of contrail cirrus," *Nature Communications*, no. 9, 2018.
- [69] G. F, "Design Evaluation / DOC," HAW-Hamburg, 2009. [Online]. Available: https://www.fzt.haw-hamburg.de/pers/Scholz/HOOU/AircraftDesign_14_DOC.pdf. [Accessed 18 August 2022].
- [70] P. J. Mukhopadhyaya and P. D. Rutherford, "PERFORMANCE ANALYSIS OF EVOLUTIONARY HYDROGEN-POWERED AIRCRAFT," ICCT, 2022.
- [71] D. S. A. Johannig, "EVALUATION OF WORLDWIDE NOISE AND POLLUTANT EMISSION COSTS FOR INTEGRATION INTO DIRECT OPERATING COST METHODS," Hamburg University of Applied Sciences, Hamburg, 2012.
- [72] Oxford institute for Energy Studies, "Path to hydrogen competitiveness: A cost perspective," Hydrogencouncil, Oxford, 2020.
- [73] E. Penrod, "Green hydrogen prices have nearly tripled as energy costs climb: S&P," 21 07 2022. [Online]. Available: <https://www.utilitydive.com/news/green-hydrogen-prices-global-report/627776/>.
- [74] M. E, R. F and G. B, "Techno-economic data for a multi-model approach to decarbonisation of the Irish private car sector," School of Engineering, University College Cork, Cork, Irland, 2017.
- [75] I. v. Halm, "Europe could have a clean power system at no extra cost by 2035," *power-technology.com*, 6 July 2022. [Online]. Available: <https://www.power-technology.com/analysis/europe-could-have-a-clean-power-system-at-no-extra-cost-by-2035/>. [Accessed 22 August 2022].
- [76] N. Pocard, "Fuel Cell Price to Drop 70-80% as Production Volume Scales," 01 02 2022. [Online]. Available: <https://blog.ballard.com/fuel-cell-price-drop>.

7 Appendix A – Three Side View



8 Appendix B -Technical Summary

Academy: Aircraft Design Challenge 2022 – Summary of technical data

1. General

Name of aircraft	HAIQU
University	University of Stuttgart
Team members	Jona Eissele, Stefan Lafer, Cristian Mejía-Burbano, Julian Schließus, Tristan Wiedmann
Supervisor	Prof. Dr. Andreas Strohmayer, M. Sc. Jonas Mangold

2. Masses

Maximum take-off mass	19 300 kg
Operating mass empty	13 200 kg

3. Fuselage

Length, width, height	25.3 m, 31.5 m, 7.1 m
No. of rows and seat configuration	13 rows total; 12 rows 2-2, last row 2-0

4. Aerodynamics

Wing area	54.2 m ²
Wing span	28.5 m
Wing loading	356.1 kg/m ²
Aspect ratio	15
Wetted area wing	97 m ²
Wetted area fuselage	208 m ²
Total wetted area	331 m ²
(L/D) in cruise (also specify altitude and TAS)	12.9 @ FL170, 298 kt

(L/D) max in cruise	18.3
Max. wing lift coefficient (take-off and landing configuration)	T/O 2.3, LDG 2.7

5. Static Margin

Minimum static margin	15 %MAC
Maximum static margin	33 %MAC

6. Propulsion System

Type of hybrid-electric architecture	Fuel cell “Battery Boosted” serial hybrid
No. of conventional engines and propulsive power of one engine	0 x 0 kW
No. of electrical motors and propulsive power of one motor	4 x 960 kW
Propeller efficiency in cruise	89 %
Overall conventional propulsive power	0 kW
Overall electrical propulsive power	3840 kW
Overall installed propulsive power	3840 kW
Overall static thrust	101 kN
Overall maximum thrust in cruise	22 kN
Power loading	20.3 W/N

7. Energy System

Primary energy source type	Liquid Hydrogen
Max. amount of primary energy	417 kg
Type(s) of secondary energy storage installed	LFP Battery
Secondary energy storage mass	1950 kg
Secondary energy storage capacity	204 kWh
Specific energy of secondary energy (cell and pack)	Cell 0.14 kWh/kg, Pack 0.105 kWh/kg
Peak power for secondary energy source	2900 kW, limited to 429 kW
Specific power of secondary energy (cell and pack)	Cell 2 kW/kg, Pack 1.5 kW/kg
For battery, maximum C-rate	2.0 1/h
Energy Management Strategy (Power split, i.e. power from secondary energy source divided by total power from all energy sources in every flight segment)	Taxi 0.00, T/O 0.12, CLB 0.1, CRZ 0.00, DES -0.61, APP -0.10, CLB_res 0.10, CRZ_res 0.10, DES_res -0.61, APP_res -0.1

8. Maximum Range Mission

Fuel mass for trip	295 kg
Energy for trip (secondary energy source(s) only)	75 kWh
Emissions for trip (CO ₂ and NO _x)	0 kg CO ₂ , 0 kg NO _x
Fuel mass for reserve	122 kg
Energy for reserve (secondary energy source(s) only)	0 kWh
Emissions for reserve (CO ₂ and NO _x)	0 kg CO ₂ , 0 kg NO _x

9. DOC Benchmark Mission

Fuel mass for trip	172 kg
Energy for trip (secondary energy source(s) only)	75 kWh

Emissions for trip (CO ₂ and NO _x)	0 kg CO ₂ , 0 kg NO _x
Fuel mass for reserve	128 kg
Energy for reserve (secondary energy source(s) only)	0 kWh
Emissions for reserve (CO ₂ and NO _x)	0 kg CO ₂ , 0 kg NO _x

10. Direct Operating Costs

DOC fuel	4.71 EUR/(100 passenger km)
DOC electric energy	0.12 EUR/(100 passenger km)
DOC maintenance	4.51 EUR/(100 passenger km)
DOC fees	11.67 EUR/(100 passenger km)
DOC personnel	1.24 EUR/(100 passenger km)
DOC capital	4.20 EUR/(100 passenger km)
DOC total	26.46 EUR/(100 passenger km)

11. Aircraft Performance

Take-off distance at MTOM, ISA, SL	980 m
Landing distance at MLM, ISA, SL	775 m
Maximum rate of climb at MTOM, ISA, SL	2400 ft/min
Climb gradient with OEI at MTOM, ISA, SL	5.1 %
Climb gradient with OEI at MTOM, ISA +28, 7316 ft	-0.4 %
Cruise altitude	17 000 ft
Cruise speed and Mach	298 kts, 0.48 Ma